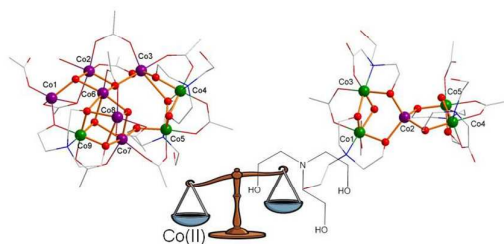




**Switching nuclearity and Co(II) content through
stoichiometry adjustment: {Co^{II}6Co^{III}3} and
{Co^{II}Co^{III}4} mixed valent complexes and their magnetic
properties study**

Journal:	<i>Dalton Transactions</i>
Manuscript ID:	DT-ART-10-2014-003034.R2
Article Type:	Paper
Date Submitted by the Author:	01-Dec-2014
Complete List of Authors:	Funes, Alejandro; Universidad de Buenos Aires, DQAQF/INQUIMAE Carrella, Luca; University of Mainz, Institute of inorganic and analytical chemistry Sorace, Lorenzo; Universit� di Firenze, Rentschler, Eva; Uiversity of Mainz, Institute of Inorganic Chemistry Albores, Pablo; Universidad de Buenos Aires,

Controlling Co^{II} content in polynuclear systems: $\{\text{Co}^{\text{II}}_6\text{Co}^{\text{III}}_3\}$ and $\{\text{Co}^{\text{II}}\text{Co}_4^{\text{III}}\}$ mixed valent complexes with distinctly magnetic behaviour are reported.



Switching nuclearity and Co(II) content through stoichiometry adjustment: $\{\text{Co}^{\text{II}}_6\text{Co}^{\text{III}}_3\}$ and $\{\text{Co}^{\text{II}}\text{Co}_4^{\text{III}}\}$ mixed valent complexes and their magnetic properties study

Alejandro V. Funes^[a], Luca Carrella^[b], Lorenzo Sorace^[c], Eva Rentschler^[b] and Pablo Alborés^{[a]*}

[a] Departamento de Química Inorgánica, Analítica y Química Física/ INQUIMAE (CONICET), Facultad de Ciencias Exactas y Naturales Universidad de Buenos Aires, Pabellón 2, Ciudad Universitaria, C1428EHA Buenos Aires, Argentina
Fax: +5411 / 4576-3341
E-mail: albores@qi.fcen.uba.ar

[b] Institute of Inorganic and Analytical Chemistry, Johannes Gutenberg - University of Mainz, Duesbergweg 10-14 D-55128 Mainz-Germany.
Fax: +49 6131 / 39-23922

[c] Dipartimento di Chimica "U. Schiff" and UdR INSTM, Università di Firenze, Via della Lastruccia 3, Polo Scientifico, 50019, Sesto Fiorentino, Firenze, Italy.
Fax: +39-055-4573372

Keywords

Cobalt- polynuclear complexes- magnetic properties- DFT- EPR

Abstract

We are reporting two new mixed valent Co(II)/Co(III) polynuclear complexes, bearing different amount of Co(II) ions in their cores, $\{\text{Co}^{\text{II}}_6\text{Co}^{\text{III}}_3\}$ and $\{\text{Co}^{\text{II}}\text{Co}_4^{\text{III}}\}$ through employment of the multidentate triethanolamine (teaH_3) ligand under different stoichiometric ratios. We are presenting a complete picture of the magnetic behaviour of both complexes through a combined usage of susceptibility, magnetization and X-band EPR data as well as Broken-Symmetry DFT calculations. Compound 1 shows an atypical spin-only behaviour,

probably due to the presence of four and five coordinated Co(II) sites as well as highly distorted six coordinated Co(II) ions, promoting high degree of orbital contribution quenching. Through usage of a simplify exchange coupling scheme and relying on DFT based magneto-structural correlation we have been able to explain the observed diamagnetic ground state. Concerning compound 2, DC magnetic data supported by X-band EPR measurements; suggest the existence of anisotropy with a zero-field splitting parameter D , at least in the range $2\text{-}10\text{ cm}^{-1}$. In agreement with this description, slow relaxation of magnetization is observed after applying a small external magnetic field, under AC measurements. Field and temperature dependence of characteristic relaxation time establishes a thermal barrier for magnetization reversal of about 25 cm^{-1} , which is in good agreement with the energy splitting of the $|\pm 1/2\rangle$ and $|\pm 3/2\rangle$ doublets established from static magnetic measurements.

Introduction

Polynuclear transition metal complexes bearing paramagnetic ions continue to be a research target in molecular magnetism, as they can be suitable for investigating slow relaxation of the magnetization phenomena (single molecule magnet behaviour, SMM)¹ but also as promising units for molecular refrigerants² as well as suitable models in the field of molecular spintronics³.

In comparison with the well extended and explored cluster chemistry including manganese and iron in different oxidation states as 3d ions⁴, the number of hydroxide- and/or carboxylate-bridged cobalt clusters for which the magnetic properties have been thoroughly investigated is still limited⁵. This is probably due to the problems faced to deeply understand their magnetic behaviour, largely influenced by the strong angular momentum appearing in the ground state at first order⁶. More recently, mirroring the development of single-ion-magnets (SIM) based on lanthanides⁷, examples based on mononuclear complexes containing 3d metal ions with unquenched orbital momentum have been reported⁸, most of them containing Co(II) ions. The driving force for this new approach is the possibility of exploiting the huge single-ion anisotropy of these systems which produces a large barrier to the magnetization reorientation.

In the case of mixed-valence cobalt polynuclear complexes, since low-spin d^6 cobalt(III) is diamagnetic, the interesting magnetic properties arise from cobalt(II) alone, which is a paramagnetic ion usually exhibiting a strong anisotropy^{6b,6c}. In this context, mixed-valency constitutes an alternative route to control the Co(II) content in cobalt polynuclear systems, but preserving the molecular topology diversity. An efficient synthetic procedure, in the case of mixed valence clusters, consists in the slow oxidation of Co(II) by air, in the presence of carboxylate source and other auxiliary ligand with bridging ability.

Following our research project in the field of polynuclear cobalt complexes⁹, we have explored the reaction of triethanolamine (teaH₃) with a cobalt(II) pivalate (trimethylacetate=piv) precursor. Employing acetonitrile as reaction solvent, in the presence of triethylamine as a base, two widely differing in nuclearity and Co(II) content, new mixed valent polynuclear cobalt complexes were isolated: a nonanuclear [Co^{II}₆Co^{III}₃(piv)₁₀(tea)(teaH)₂(OH)₄(H₂O)] (**1**) and a pentanuclear [Co^{II}Co^{III}₄(piv)₄(teaH)₂(bicH)₂(OH)₂] (**2**), (H₃bic=bicine, 2-(Bis(2-hydroxyethyl)amino)acetic acid). Here in we report its structural characterization and their magnetic properties carefully analysed.

Results and Discussion

Synthesis and structural characterization

As has already previously shown, the starting cobalt (II) complex, [Co₂(μ-OH₂)(μ-Piv)₂(Piv)₂(HPiv)₄], can re-arrange in solution to afford higher nuclearity cobalt compounds and in this sense stands as a highly versatile synthetic precursor⁹⁻¹⁰. In the presence of the additional ligand teaH₃ (triethanolamine) (Scheme 1) and a suitable base (in this case, triethylamine), its reaction in acetonitrile at room temperature affords two different polynuclear mixed valent complexes. When the teaH₃:Co molar ratio is kept low, the nonanuclear compound **1** is obtained, while increasing the teaH₃ content affords the pentanuclear compound **2**. Both complexes are obtained in crystalline form and moderate yields. As no air exclusion was performed, these new compounds exhibit mixed valent {Co^{II}_xCo^{III}_y} cores, where partial cobalt oxidation presumably proceeded by means of atmospheric oxygen. Interestingly, the increased number of teaH₃ ligands in the final compounds, mirrors an increased Co(III) content and hence a decreased Co(II) one. In fact,

complex **2** bears a unique Co(II) ion with a $\{\text{Co}^{\text{II}}\text{Co}^{\text{III}}_4\}$ core, in comparison with the six Co(II) sites found in compound **1**, which exhibits a $\{\text{Co}^{\text{II}}_6\text{Co}^{\text{III}}_3\}$ core (Figures 1 and 2).

Surprisingly, when looking at compound **2** molecular structure, two coordinated bicine ligands (Scheme 1) are found, instead of the expected triethanolamine ligands. Most probably, a metal assisted oxidation of teaH₃ took place affording the final transformed ligand bicine. It should be remarked that this preparation is completely reproducible, with reasonable yields, affording always the same final structure which includes the transformed bicine ligand.

Compound **1** crystallizes in a *P*-1 triclinic space group with a unique molecule in the asymmetric unit and two additional crystallization water solvent molecules. The overall molecular structure shows a rather atypical topology, resembling a Co₇ ring arrangement with the remaining two Co sites included as part of a nested cubane [Co₄O₄] moiety (Figure 1).

The $\{\text{Co}^{\text{II}}_6\text{Co}^{\text{III}}_3\}$ core bears nine crystallographic independent Co ions, with different coordination numbers, Co(2), Co(4), Co(5), Co(6), Co(7), Co(8) and Co(9) in octahedral environment, Co(1) in tetrahedral environment and Co(3) in square pyramidal environment. This nonanuclear metallic core is held by two Htea²⁻ ligands (doubly deprotonated) binding in the [3.221] mode (according to Harris notation¹¹), a tea³⁻ ligand (fully deprotonated) binding in the [5.3321] mode, eight [2.11] mode (μ_2) pivalates ligands, four [3.1] mode (μ_3) hydroxo ligands and it is finally capped by a κ^2 -pivalate, a κ^1 -pivalate and an aqua ligand. The $\{\text{Co}^{\text{II}}_6\text{Co}^{\text{III}}_3\}$ formal oxidation-state description is strongly supported by bond distances. Octahedral Co-O bond distances fall into two well-separated groups with distances involving Co(4), Co(5) and Co(9) ranging between 1.845(7)-1.946(9) Å, that correspond to Co(III) sites and those from Co(2), Co(6), Co(7) and Co(8) ranging between 1.994(7)-2.285(8) Å; corresponding to Co(II) sites. The other Co(II) sites undoubtedly correspond to the four coordinated Co(1) and five-coordinated Co(3) sites.

Compound **1** complicated structure can be better understood in terms of smaller cores (Figure 1) with already known typical arrangements: the Co(6)-Co(7)-Co(8)-Co(9) cubane core; the Co(1), Co(2), Co(3), Co(6) alternated-wings butterfly core and the Co(4), Co(5) μ -hydroxo- μ -carboxylate dinuclear unit. These three different cores are connected among them as following described. Co(6) constitutes one vertex of the cubane core and at the same time one body member of the butterfly core while a single alkoxo bridge from one teaH²⁻ ligand constitutes an additional connection between cubane and butterfly cores. The $\{\text{Co}(4)\text{-Co}(5)\}$

dinuclear core is connected at both sides to the cubane and butterfly cores through μ -alkoxo (from teaH^{2-} ligand) and μ -pivalate bridges.

Short intra-molecular contacts can be found involving both μ_3 -hydroxides of the cubane core (O114 and O116) and adjacent teaH^{2-} and pivalate ligands (O113 and O16 respectively). Hydrogen bonding between these moieties are clearly present (see ESI). An additional intra-molecular H-interaction can be observed between the terminal aqua and the close terminal κ^1 -pivalate ligand (O118 and O210 respectively).

When looking at other reported Co_9 compounds based on carboxylato and/or alkoxo skeletons, over a list of about fifteen reported structures¹², only one related compound is found with formula $[\text{Co}^{\text{II}}_9(\text{piv})_{12}(\text{OH})_6((\text{CH}_3)_2\text{CO})]^{12a}$. In this compound the cubane core is completely opened at one corner and the butterfly core exhibits smaller body-wing angles approaching also an opened cubane like structure.

Regarding the crystal packing, a complex H-bonding network, involving the water solvent molecules and the terminal aqua and pivalate ligands at one side, and the free alcohol arm of teaH^{2-} ligand at the opposite side, held molecules packed in columns running along *a* and *b* axis (see ESI). A four molecules arrangement constitutes the main H-bonding inter-molecular network pattern (see ESI). As a result of this interacting pattern, the closest inter-molecular Co...Co distance is 8.668(2) Å between Co(4) and Co(8) of adjacent molecules.

Compound **2** crystallizes in a monoclinic *P21/n* cell. The asymmetric unit consists of one complex **2** moiety with an acetonitrile and two water solvent molecules. The molecular structure of **2** is built up by a central distorted tetrahedral cobalt ion with the side capping of two dinuclear octahedral cobalt cores (Figure 2). The overall structure is held together through two teaH^{2-} ligands binding in a [3.221] mode, two bicH^{2-} ligands in a [2.211] mode, two [2.11](μ_2) pivalates and one μ_3 - and two μ_2 -hydroxide ligands. Final Co coordination spheres completeness is achieved through two κ^1 -pivalate ligands. Co-O distances fall into well-separated groups with distances involving the octahedral Co sites ranging between 1.867 – 1.981 Å, and those from the tetrahedral Co site ranging between 2.004 – 2.041 Å. From this metric, all six coordinated Co(1), Co(3), Co(4) and Co(5) correspond to Co(III) ions, remaining then a unique Co(II) ion, Co(2), affording an overall $\{\text{Co}^{\text{II}}\text{Co}^{\text{III}}_4\}$ mixed valent core. A closer inspection to this core evidences that both $\{\text{Co}^{\text{III}}_2\}$ units are essentially identical, in spite of not being crystallographically related moieties. They are composed of a triple μ -

hydroxo- μ -alkoxo- μ -carboxylato bridge with very similar bridging angles and distances (see ESI). Both dinuclear moieties clamp at both sides the central Co(II) site through the not bridging alkoxyde O atoms of the teaH^{2-} and bicH^{2-} ligands creating the tetrahedral environment. Notably, one of the $\{\text{Co}_2\}$ μ -hydroxo oxygen atoms, O(19) appears at a rather short distance from the central Co(II) ion, Co(2)-O(19), 2.360(3) Å perturbing and distorting the tetrahedral arrangement (one of the tetrahedral, O(25)-Co(2)-O(27), angles deviates to 94.4(1) degrees) (see ESI).

A very similar $\{\text{Co}^{\text{II}}\text{Co}^{\text{III}}_4\}$ compound has been previously reported, based on a teaH_3 derivative and acetate ligands and without hydroxide bridges¹³. However in this example, the central Co(II) site has no additional oxygen atoms at short distances (the shortest Co-O remote distance is above 2.6 Å, bearing a well defined tetrahedral environment).

An extremely complicated H-bonding network is observed in the crystal packing of compound **2** molecules mainly involving the water solvent molecules and the free, not coordinating oxygen atoms of teaH^{2-} and bicH^{2-} ligands. As a result, complex **2** molecules arrange in columns running along the *b*-axis (see ESI), with the shortest inter-molecular (intra-columnar) Co...Co distance of 7.931(1) Å between Co(3).....Co(4)'. The shortest inter-columnar Co....Co distance of 10.804 Å is observed between Co(1).....Co(5)'.

Magnetic properties

Variable-temperature (2–300 K) DC magnetic susceptibility data at 0.1T were recorded for complexes **1** and **2** (Figure 3). The $\chi_m T$ product of **1** at 300 K of 17.0 $\text{cm}^3\text{mol}^{-1}\text{K}$ is clearly higher than the spin-only value ($g=2.0$) expected for six non-interacting $S=3/2$ centers (11.25 $\text{cm}^3\text{mol}^{-1}\text{K}$). In order to achieve the observed $\chi_m T$ value at 300K the *g* value should be close to a 2.45 value. It is well known the orbital contribution to the magnetic moment in Co(II) ion in an octahedral field^{6b}, however under this condition $\chi_m T$ at room temperature normally exhibits values compatible with a *g* close to 3.0^{9b-d}. Hence, in this case and at this point, there is a first hint suggesting a considerable quenching of the orbital contribution to the magnetic moment. The continuous decrease in $\chi_m T$, approaching a zero value at low temperature, evidences overall dominant anti-ferromagnetic interactions among Co(II) sites if the orbital contribution, as suspected, is considered almost negligible.

In the case of complex **2**, bearing a unique Co(II) ion and consequently behaving like a mononuclear Co complex in terms of magnetic properties, the $\chi_m T$ value at 300 K is 3.2 cm³mol⁻¹K. The latter is higher than the spin-only value ($g=2.0$) expected for an $S=3/2$ center (1.875 cm³mol⁻¹K). However with a g value close to 2.6 it is possible to match the experimental data. This still high g value suggests that some orbital contribution at first order remains, even when a complete quenching of the orbital contribution is expected for a strict tetrahedral environment (4A_2 ground state). This discrepancy, maybe reflecting the direct influence of the O(19) atom at short contact distance from the Co(II) ion which perturbs the tetrahedral environment. When looking at the complete $\chi_m T$ vs T profile, a constant value of 3.2 cm³mol⁻¹K is observed up to 30 K, where a pronounced decreasing becomes evident, most probably due to the onset of zero field splitting. Regrettably, no magnetic measurements were performed in the previously reported and closely related $\{\text{Co}^{\text{II}}\text{Co}^{\text{III}}_4\}$ compound, so no comparison can be made¹³.

We also performed magnetization data measurements at different applied external fields (1-70 kOe) in the 2-10 K temperature range. These data further proves, in the case of compound **1**, the non-magnetic ground state nature (Figure 4), as magnetization slowly and linearly increases upon cooling down to 2 K and sweeping field up to 70 kOe very far away of any saturation behaviour. In addition, a spin level crossing is observed at around 25 kOe, also supporting the non-magnetic ground state.

Regarding compound **2** magnetization data, saturation is not observed in the reduced magnetization plots, reaching a maximum value of $3.7N\beta$. This fact and the lack of a strict superposition of the isofield lines, suggest the existence of an anisotropic ground state in agreement with low temperature susceptibility data.

In order to better understand the magnetic behaviour of the reported compounds, we attempt to fit the magnetic data employing the available PHI package routines¹⁴ which rely on powder averaged full spin Hamiltonian diagonalization techniques.

Starting from the assumption that complex **1** exhibits a high degree of orbital momentum quenching, we employed a spin-only Hamiltonian considering the exchange interactions between the $S=3/2$ ions:

$$\hat{H} = -2 \sum_{i < j} J_{ij} \hat{S}_i \hat{S}_j \quad (i=1-6) \quad (1)$$

In principle from the Co(II) ions topology (Scheme 2), eight different exchange interactions constants J_{ij} should be considered. However this is clearly a non-reasonable number of fitting parameters, so a first simplification must be adopted in order to overcome this issue. Looking at the $\{\text{Co}^{\text{II}}_6\}$ interacting core, two main sub-cores can be distinguished: the butterfly moiety and the adjacent cubane one. As an approximation, only two different exchange coupling constants can be proposed within the butterfly arrangement (wing-body, J_1 and body-body, J_2 , for a perfectly symmetric arrangement). On the other hand, within the cubane arrangement, only three of the four Co sites are Co(II) ions, held in a triangular arrangement through double μ -hydroxo- μ -alkoxo bridges combinations. Two different exchange interaction constants can be proposed here, corresponding to two Co-O-Co pathways differing in Co-O-Co angles, J_3 and J_4 .

This scheme affords, as the most complete sensible approximation, a maximum of four exchange interaction constants in order to fit magnetic data (Scheme 2). However, we found enough employing only a two exchange constants model to simultaneously fit susceptibility and magnetization data with reasonable agreement. In fact, as the non-magnetic ground state nature imposes dominant anti-ferromagnetic wing-body exchange interactions within the butterfly core, the body-body exchange interaction remains largely undefined. Hence it is not possible to include it in the modelling. As a forth-coming consequence, it becomes also enough to set only one dominant exchange interaction within the cubane embedded trinuclear core to properly account for all experimental data fitting. Inclusion of the other formerly proposed exchange constants in the model does not improve overall data fitting.

The obtained values for the exchange constants arising from data fitting (Figures 3 and 4) are listed in Table 1. The isotropic g value obtained of 2.59 ± 0.01 , confirms the starting perception of orbital momentum quenching in this compound, even if still appears a little bit higher than expected for a pure spin $S=3/2$ under a perturbative approach. With these parameters an $S=0$ ground state is obtained with an $S=1$ excited state at only 2.7 cm^{-1} , responsible of the level crossing observed in the magnetization plots at *ca.* 22 kOe (see ESI).

In order to gain a deeper insight into the origin of the isotropic anti-ferromagnetic exchange interactions between the Co(II) ions in compound **1**, we performed broken-symmetry DFT calculations to evaluate the magnitude of the exchange coupling constants employing the hybrid B3LYP functional and a valence core big size (TZP) basis set. This approach has been

previously proved successful when applied to close related systems^{4y,9a,9d,15}. The calculation allows obtaining the eight possible exchange coupling constants which are not possible to discriminate from experimental data alone. The obtained calculated values extracted from the energies of the eight broken-symmetry and the high spin states (see ESI) are listed in Table 1. They compare in excellent way with both experimental exchange coupling constants magnitudes when making the average of the different J values to match the experimental modelling.

Most of the previously reported Co(II) polynuclear complexes with related bridging ligands like alkoxide, hydroxide, oxo and aqua showing ferromagnetic interactions have Co-O-Co angles well below 100°, while those exhibiting anti-ferromagnetic interactions have Co-O-Co angles well above this threshold^{10b,10c,16}. Due to the usual complexity of local symmetry over Co(II) sites in these systems and the onset of strong orbital momentum contribution, it is not straightforward to convincingly rationalize this magneto-structural aspects and there is still not a definite picture about this issue. However and notably, in this example where orbital contribution appears highly quenched and there are several and structural different Co(II) exchange interactions included into the same compound, it is possible to look at a magneto-structural correlation arising from DFT calculated exchange interaction parameters. In fact, it is found a clear correlation between the J values and the corresponding Co-O-Co bridging angles (in the case of doubly bridging O, the mean value was considered) (Figure 5). When trying a correlation with the Co-O-Co through bonds distance, it completely failed. The experimental values, once averaged the all involved angles, enter in this correlation, as expected from their good agreement with the DFT calculated ones. From this data set correlation, the critical angle where J changes sign is found to be 98°, in agreement with the general previous observation in related Co(II) polynuclear compounds^{10b,10c,16}.

In overall, complex **1** constitutes a rare example of a polynuclear cobalt complex where magnetic properties can be completely understood, exclusively, under a spin-only formalism.

Magnetic properties of compound **2** appears simplified due to the presence of a unique Co(II) site in a certainly perturbed tetrahedral environment. Susceptibility and magnetization data fitting can be performed through a $S=3/2$ Hamiltonian with an axial ZFS term:

$$\hat{H} = g_{iso}\beta\overline{H}\hat{S} + D(\hat{S}_z^2 - \frac{5}{4}) \quad (2)$$

When attempting a simultaneous data fit (susceptibility+magnetization), the following common best fitting parameters set is obtained: $g_{\text{iso}}=2.59\pm 0.01$ and $|D|=2.1\pm 0.1 \text{ cm}^{-1}$ (Figures 3 and 4). However, in this case the D parameter is poorer defined from magnetization data than from susceptibility one. In fact, best fitting parameters arising only from $\chi_m T$ vs T data are: $g_{\text{iso}}=2.61\pm 0.01$ and $|D|=8.7\pm 0.5 \text{ cm}^{-1}$ while the ones arising only from magnetization data are: $g_{\text{iso}}=2.68\pm 0.07$ and $|D|=3\pm 10 \text{ cm}^{-1}$. Inspection of g_{iso} vs D residual error surface from magnetization data fitting clearly evidences a great uncertainty in D parameter (see ESI). In overall, it seems clear the existence of a sizeable ZFS term, with $|D|$ at least in the range 2-10 cm^{-1} while the obtained g_{iso} value is somehow higher than the normally observed value for tetrahedral Co(II) sites with completely quenched orbital contribution. As already suggested, most probably, the perturbation of the tetrahedral environment by the short contact oxygen atom, O(19), from the neighbouring hydroxo ligand has something to do with this observation.

With the aim of further testing the whole set of parameters describing magnetic data of compound **2** we performed powder X-band EPR (9.397 GHz) measurements at 1.5K and 5K (Figure 6). The spectra resembles a $S_{\text{eff}}=1/2$ with apparent axial anisotropy, with broad resonances at *ca.* 310 Oe, and 125 Oe. The approximate g^{eff} values corresponding to these resonance fields are $g^{\text{eff}}_{\perp} \sim 5.4$ and $g^{\text{eff}}_{\parallel} \sim 2.2$, in agreement with the expected results for a $S=3/2$ with D parameter larger than the microwave energy in full agreement with susceptibility and magnetization data ($g^{\text{eff}}_{\parallel}=g_{\parallel}$; $g^{\text{eff}}_{\perp}=2g_{\perp}$; hence for g close to 2.6, $g^{\text{eff}}_{\perp} \sim 5.4$ and $g^{\text{eff}}_{\parallel} \sim 2.6$). However the sign of this parameter remains undefined under this X-band measurement. Broadening of lines, most probably due to unresolved hyperfine interactions, makes a precise spectrum simulation difficult. Nevertheless, a reasonable simulation can be obtained with the following parameters: $|E/D|=0.15$, $g=2.15$ and employing g - and H - strain to account for the asymmetric lines broadening¹⁷. This results prove the existence of a high degree of rhombicity, not completely unexpected when looking at the coordination environment of the Co(II) site (*cf.* structural discussion). An equivalent simulation can be also obtained under the $S_{\text{eff}}=1/2$ picture with the following parameters: $g^{\text{eff}}_{\text{x}}=3.2$, $g^{\text{eff}}_{\text{y}}=5.1$, $g^{\text{eff}}_{\text{z}}=2.0$ (see ESI).

In order to test for possible slow magnetization relaxation behaviour, in view of the existence of a considerable ZFS contribution, alternating-current (AC) magnetic susceptibility of **2** was investigated under zero and non-zero applied static fields, respectively. Although no peaks of χ_m'' are observed under zero external DC magnetic field even at the highest

achievable frequency ($\nu = 1500$ Hz), non-zero χ_m'' signals appeared when an external DC magnetic field was applied, suggesting the onset of a slow relaxation of the magnetic moment. A field scanning at 2K of the out of phase susceptibility response up to 3 kOe at different frequencies suggests maximum values between 1400 and 2600 Oe (see ESI). Hence, we further performed a complete temperature and frequency dependent AC measurements at these two external applied magnetic DC fields. A clear maximum in the out of phase signal is observed below 12 K at both fields, which shifts with frequency and temperature, evidencing an SMM like slow relaxation of magnetization (Figure 7 and ESI).

Cole- Cole plots can be well fitted with a single characteristic relaxation time, in the 2-6 K range at both DC applied fields and at 2K between 400-3000 Oe DC applied fields (Figure 8 and ESI), employing a generalized Debye model¹⁸:

$$\chi_{ac} = \chi_s + \frac{\chi_T - \chi_s}{1 + (i\omega\tau)^{(1-\alpha)}} \quad (3)$$

From these fittings the characteristic relaxation time temperature and field dependence at 2K, can be analysed in order to extract magnetization relaxation dynamic parameters, including thermal barrier for magnetization reversal. The field dependence of the relaxation times can be reasonably fitted employing the following equation suitable for a Kramer ion¹⁷:

$$\frac{1}{\tau} = A_1 H^4 T + \frac{B_1}{1 + B_2 H^2} \quad (4)$$

where the first term corresponds to the direct relaxation process while the second one is related to the temperature independent quantum tunnelling relaxation process. The best parameters found are: $A_1 = 4.8 \times 10^{-13} \text{ s}^{-1}\text{K}^{-1}\text{Oe}^{-4}$; $B_1 = 478 \text{ s}^{-1}$ and $B_2 = 1.1 \times 10^{-6} \text{ Oe}^{-2}$ (Figure 9).

On the other hand, it is possible to fit the relaxation time temperature dependence at both explored fields, 1400 and 2600 Oe, by adding an additional term that takes into account the thermal activated Orbach process¹⁷:

$$\frac{1}{\tau} = \frac{1}{\tau_0} \exp\left(-\frac{U_{\text{eff}}}{kT}\right) + \frac{1}{\tau_{QT}} + CT \quad (5)$$

As it is difficult to extract a reliable value for the direct relaxation component, this term was fixed employing the parameter A_1 arising from the field dependence of the relaxation times, considering that $C = A_1 H^4$. The final parameters arising from temperature dependence data are: $U_{\text{eff}} = 25 \text{ cm}^{-1}$; $\tau_0 = 6.0 \times 10^{-7} \text{ s}$; $\tau_{QT} = 5.7 \times 10^{-3} \text{ s}$ for $H_{\text{DC}} = 1400 \text{ Oe}$ and $U_{\text{eff}} = 27 \text{ cm}^{-1}$; $\tau_0 = 3.5 \times 10^{-7} \text{ s}$; $\tau_{QT} = 7.9 \times 10^{-3} \text{ s}$ for $H_{\text{DC}} = 2600 \text{ Oe}$ (Figure 9 and ESI). When comparing these tunnelling relaxation times with parameters B_1 and B_2 arising from field dependent data, a good agreement is found. Notably, the thermal barrier values obtained from these dynamic magnetic data are close to the energy difference between the $|\pm 1/2\rangle$ and $|\pm 3/2\rangle$ states given by the magnitude $2|D|$ which equals *ca.* 16 cm^{-1} from the upper bound obtained from DC magnetic data. All evidences point to a well established slow relaxation of magnetization in this compound as already previously observed in other Co(II) mononuclear systems^{8a, c-e, g, i-m}.

Conclusions

By adjusting stoichiometric ratios of reactants, we have been able to isolated two different mixed valent Co(II)/Co(III) polynuclear complexes, bearing different amount of Co(II) ions in their cores, $\{\text{Co}^{\text{II}}_6\text{Co}^{\text{III}}_3\}$ (**1**) and $\{\text{Co}^{\text{II}}\text{Co}^{\text{III}}_4\}$ (**2**), and hence showing different magnetic behaviour. We have given a complete picture of the magnetic behaviour of both complexes through a combined usage of susceptibility, magnetization and EPR data as well as Broken-Symmetry DFT calculations. In the case of compound **1**, we have supported a magnetic data interpretation that shows an atypical spin-only behaviour, probably due to the presence of four and five coordinated Co(II) sites as well as highly distorted six coordinated Co(II) ions, promoting high degree of orbital contribution quenching. Through a simplify exchange coupling scheme and relying on DFT based magneto-structural correlation we have been able to explain the observed diamagnetic ground state. Concerning compound **2**, which can be treated as a Co(III) decorated mononuclear Co(II) ion, magnetic modelling was performed by means of a conventional spin-only Hamiltonian due to the tetrahedral

environment observed, which in principle avoids orbital momentum contributions. DC magnetic data supported by X-band EPR measurements; suggest a zero-field splitting parameter $|D|$, at least in the range $2\text{-}10\text{ cm}^{-1}$. In agreement with this description, slow relaxation of magnetization is observed after applying a small external magnetic field, under AC measurements. Field and temperature dependence of characteristic relaxation time establish a thermal barrier for magnetization reversal of about 25 cm^{-1} , which is in good agreement with the energy splitting of the $|\pm 1/2\rangle$ and $|\pm 3/2\rangle$ doublets established from static magnetic measurements.

In summary, we have shown that it is possible tailoring the Co(II) content within polynuclear mixed valent cobalt compounds and hence, promoting distinct magnetic behaviour. In the case of complex **2**, we found a new example where single ion slow relaxation of magnetization is observed for a Co(II) species, in this case embedded in a more complex diamagnetic polynuclear backbone.

Experimental Section

Material and physical measurements: $[\text{Co}_2(\mu\text{-OH}_2)(\mu\text{-piv})_2(\text{piv})_2(\text{Hpiv})_4]$, piv=trimethylacetate, was prepared following a previously reported procedure^{10d}. All other chemicals were reagent grade and used as received without further purification. Elemental analysis for C, H and N were performed with a Carlo Erba 1108 analyzer.

Synthesis of complexes:

$[\text{Co}^{\text{II}}_6\text{Co}^{\text{III}}_3(\text{piv})_{10}(\text{tea})(\text{teaH})_2(\text{OH})_4(\text{H}_2\text{O})] \cdot 2\text{H}_2\text{O}$ (**1**) $[\text{Co}_2(\mu\text{-OH}_2)(\mu\text{-piv})_2(\text{piv})_2(\text{Hpiv})_4]$ (95 mg, 0.1 mmol) was dissolved in 10 mL of acetonitrile, followed by the addition of triethanolamine (29.9 mg, 0.2 mmol) and triethylamine (61 mg, 0.6 mmol) dissolved in 10 mL of acetonitrile; affording a purple solution. The latter was then stirred for an hour, filtered and allowed to stand sealed at room temperature. Within 3-4 weeks purple blocks of **1** crystallized in approximate yield of 22.7 % (10.6 mg). They were filtered, washed with acetonitrile and air dried. Anal. Calcd. for $\text{Co}_9\text{C}_{68}\text{H}_{138}\text{N}_3\text{O}_{36}$ (2104.2) C, 38.8; H, 6.6; N, 2.0. Found: C, 38.9; H, 6.5; N, 2.0.

[Co^{II}Co^{III}₄(piv)₄(teaH)₂(bicH)₂(OH)₂].4H₂O·CH₃CN (2) [Co₂(μ-OH₂)(μ-piv)₂(piv)₂(Hpiv)₄] (97 mg, 0.1 mmol) was dissolved in 10 mL of acetonitrile, followed by the addition of triethanolamine (59.8 mg, 0.4 mmol) dissolved in 10 ml of acetonitrile; affording a purple solution. The latter was then stirred for an hour, filtered and allowed to stand sealed at room temperature. Within 3-4 weeks red needles of **2** crystallized in approximate yield of 50.1 % (29.2 mg). They were filtered, washed with acetonitrile and air dried. Anal. Calcd. for Co₅C₄₆H₉₇N₅O₂₈ (1463.1) C, 37.8; H, 6.7; N, 4.8. Found: C, 37.9; H, 6.5; N, 4.8.

Magnetic measurements: Magnetic measurements were performed with a Quantum Design MPMS-XL-7 SQUID magnetometer. All experimental magnetic data were corrected for the diamagnetism of the sample holders and of the constituent atoms (Pascal's tables). AC measurements were performed at driving frequencies ranging 10 to 1400 Hz with AC field amplitude of 3 Oe in DC fields ranging 0-30 kOe. X-Band EPR spectra were measured with a Bruker Elexsys E500 spectrometer equipped with a liquid ⁴He flux cryostat (ESR900, Oxford Instruments) to measure at low temperatures. Simulated EPR spectra were carried out with Easyspin package¹⁹.

X-ray Structure Determination: Crystal structures of compounds **1** and **2** were determined with an Oxford Xcalibur, Eos, Gemini CCD area-detector diffractometer using graphite-monochromated Mo-*K*α radiation ($\lambda = 0.71069 \text{ \AA}$) at 298 K. Data was corrected for absorption with CrysAlisPro, Oxford Diffraction Ltd., Version 1.171.33.66, applying an empirical absorption correction using spherical harmonics, implemented in SCALE3 ABSPACK scaling algorithm²⁰. The structure was solved by direct methods with SIR97²¹ and refined by full-matrix least-squares on F^2 with SHELXL-2014²² under WinGX platform²³. Hydrogen atoms were added geometrically or from the density difference map in the case of acidic ones, and refined as riding atoms with a uniform value of U_{iso} . In the case of compound **1**, the *tert*-butyl groups of five pivalate ligands were found disordered and were refined over two split positions. Regarding compound **2**, most carbon atoms as well as the oxygen atom of the pendant arm teaH₂⁻ ligand solvent were also found disordered and were thus refined over two split positions in the case of C atoms and three split positions for the O atom. Both water solvent molecules were also found disordered and were refined over two split positions one of them fixed to a 0.5:0.5 occupancy ratio by imposed crystal symmetry. Final crystallographic

data and values of R_1 and wR are listed in Table S1 (see ESI) while the main angles and distances are listed in Table S2 (see ESI). CCDC 1026941-1026942 contains the supplementary crystallographic data for this paper. These data can be obtained free of charge from the Cambridge Crystallographic Data Center via www.ccdc.cam.ac.uk/data_request/cif.

Quantum Chemical Calculations: Density functional theory (DFT) spin-unrestricted calculations were performed using the ADF 2010.02 program²⁴ at the B3LYP level employing a frozen core TZP basis. High accuracy converged (less than 1×10^{-6} hartrees in the commutator of the Fock and the P-matrices) single point calculations at the X-ray geometries were performed in order to analyze the exchange coupling between cobalt centres. The methodology applied here relies on the broken symmetry formalism, originally developed by Noodleman for SCF methods²⁵, which involves a variational treatment within the restrictions of a single spin-unrestricted Slater determinant built upon using different orbitals for different spin. This approach has been later applied within the frame of DFT²⁶. The HS (high spin) and BS (broken symmetry) energies were then combined to estimate the exchange coupling parameter J involved in the widespread used Heisenberg-Dirac-van Vleck Hamiltonian²⁷. We have calculated the different spin topologies of broken symmetry nature (see ESI) by alternatively flipping spin on the different metal sites. The exchange coupling constants J_i can be obtained after considering the individual pair-like components spin interactions involved in the description of the different broken symmetry states. We used the method proposed by Ruiz and co-workers²⁸, where the following equation is applied:

$$E_{BS} - E_{HS} = 2J_{12}(2S_1S_2 + S_2), \quad \text{with } S_2 < S_1$$

In both cases a set of linear equations must be solved to obtain the J parameters.

Acknowledgments

We gratefully acknowledge UBA, ANPCYT and CONICET for funding resources. PA is a staff member of CONICET and AVF is a doctoral fellow of CONICET. DFT computations

were performed at the Jülich Supercomputer Center (JSC)-Germany, under the NIC project 4953.

References

1. (a) A. Venugopal, F. Tuna, T. P. Spaniol, L. Ungur, L. F. Chibotaru, J. Okuda, and R. A. Layfield, *Chem. Commun.*, 2013, **49**, 901; (b) D. Gatteschi, R. Sessoli, and J. Villain, *Molecular Nanomagnets*, Oxford University Press, 2006; (c) G. Aromi and E. K. Brechin, *Single-Molecule Magnets and Related Phenomena*, 2006, **122**, 1; (d) G. Christou, D. Gatteschi, D. N. Hendrickson, and R. Sessoli, *MRS Bull.*, 2000, **25**, 66.
2. (a) Y.-Z. Zheng, G.-J. Zhou, Z. Zheng, and R. E. P. Winpenny, *Chem. Soc. Rev.*, 2014, **43**, 1462; (b) R. Sessoli, *Angew. Chem. Int. Ed. Engl.*, 2012, **51**, 43; (c) M. Evangelisti and E. K. Brechin, *Dalton Trans.*, 2010, **39**, 4672.
3. (a) S. Sanvito, *Chem. Soc. Rev.*, 2011, **40**, 3336; (b) L. Bogani and W. Wersndorfer, *Nat. Mater.*, 2008, **7**, 179.
4. (a) R. Bagai, K. A. Abboud, and G. Christou, *Inorg. Chem.*, 2007, **46**, 5567; (b) A. M. Ako, V. Mereacre, Y. H. Lan, W. Wersndorfer, R. Clerac, C. E. Anson, and A. K. Powell, *Inorg. Chem.*, 2010, **49**, 1; (c) E. S. Koumoussi, A. Routzomani, T. N. Nguyen, D. P. Giannopoulos, C. P. Raptopoulou, V. Psycharis, G. Christou, and T. C. Stamatatos, *Inorg. Chem.*, 2013, **52**, 1176; (d) M. Murugesu, K. A. Abboud, and G. Christou, *Polyhedron*, 2004, **23**, 2779; (e) R. Bagai, K. A. Abboud, and G. Christou, *Chem. Commun.*, 2007, 3359; (f) C. M. Beavers, A. V. Prosvirin, A. V. Prosvirin, J. D. Cashion, K. R. Dunbar, and A. F. Richards, *Inorg. Chem.*, 2013, **52**, 1670; (g) T. Taguchi, M. S. Thompson, K. A. Abboud, and G. Christou, *Dalton Trans.*, 2010, **39**, 9131; (h) T. Liu, Y. J. J. Zhang, Z. M. Wang, and S. Gao, *J. Am. Chem. Soc.*, 2008, **130**, 10500; (i) K. Mason, A. Prescimone, M. Schau-Magnussen, S. Piligkos, P. Tasker, and E. Brechin, *Curr. Inorg. Chem.*, 2013, **3**, 76; (j) S. Konar, N. Bhuvanesh, and A. Clearfield, *J. Am. Chem. Soc.*, 2006, **128**, 9604; (k) R. Bagai, S. Datta, A. Betancur-Rodriguez, K. A. Abboud, S. Hill, and G. Christou, *Inorg. Chem.*, 2007, **46**, 4535; (l) A. Ferguson, J. McGregor, A. Parkin, and M. Murrie, *Dalton Trans.*, 2008, 731; (m) A. K. Boudalis, Y. Sanakis, J. M. Clemente-Juan, B. Donnadieu, V. Nastopoulos, A. Mari, Y. Coppel, J. P. Tuchagues, and S. P. Perlepes, *Chem. Eur. J.*, 2008, **14**, 2514–2526; (n)

- T. Shiga, M. Noguchi, H. Sato, T. Matsumoto, G. N. Newton, and H. Oshio, *Dalton Trans.*, 2013, **42**, 16185; (o) P. Alborés and E. Rentschler, *Eur. J. Inorg. Chem.*, 2008, **2008**, 4004; (p) S. Liu, J. M. Jia, L. Xue, Y. Cui, S.-D. Han, S.-M. Zhang, and Z. Chang, *CrystEngComm*, 2014, **16**, 5212; (q) D. Gatteschi, A. Caneschi, R. Sessoli, and A. Cornia, *Chem. Soc. Rev.*, 1996, **25**, 10; (r) T. Taguchi, W. Wersndorfer, K. A. Abboud, and G. Christou, *Inorg. Chem.*, 2010, **49**, 10579; (s) T. C. Stamatatos and G. Christou, *Philos. Trans. R. Soc. a-Mathematical Phys. Eng. Sci.*, 2008, **366**, 113; (t) T. C. Stamatatos, D. Foguet-Albiol, W. Wersndorfer, K. a Abboud, and G. Christou, *Chem. Commun.*, 2011, **47**, 274; (u) S. J. Shah, C. M. Ramsey, K. J. Heroux, J. R. O'Brien, A. G. DiPasquale, A. L. Rheingold, E. del Barco, and D. N. Hendrickson, *Inorg. Chem.*, 2008, **47**, 6245; (v) E. E. Moushi, C. Lampropoulos, W. Wersndorfer, V. Nastopoulos, G. Christou, and A. J. Tasiopoulos, *J. Am. Chem. Soc.*, 2010, **132**, 16146; (x) M. Manoli, R. Inglis, M. J. Manos, V. Nastopoulos, W. Wersndorfer, E. K. Brechin, and A. J. Tasiopoulos, *Angew. Chemie-Int. Ed.*, 2011, **50**, 4441; (y) S. Nayak, M. Evangelisti, A. K. Powell, and J. Reedijk, *Chem. Eur. J.*, 2010, **16**, 12865; (z) S. K. Langley, R. A. Stott, N. F. Chilton, B. Moubaraki, and K. S. Murray, *Chem. Commun.*, 2011, **47**, 6281; (aa) M. Manoli, A. Prescimone, R. Bagai, A. Mishra, M. Murugesu, S. Parsons, W. Wersndorfer, G. Christou, and E. K. Brechin, *Inorg. Chem.*, 2007, **46**, 6968; (ab) S. M. Taylor, G. Karotsis, R. D. McIntosh, S. Kennedy, S. J. Teat, C. M. Beavers, W. Wersndorfer, S. Piligkos, S. J. Dalgarno, and E. K. Brechin, *Chemistry*, 2011, **17**, 7521; (ac) D. Liu, Q. Zhou, Y. Chen, F. Yang, Y. Yu, Z. Shi, and S. H. Feng, *Dalton Trans.*, 2010, **39**, 5504; (ad) O. Roubeau and R. Clerac, *Eur. J. Inorg. Chem.*, 2008, 4325; (ae) S. Nayak, L. M. C. Beltran, Y. H. Lan, R. Clerac, N. G. R. Hearn, W. Wersndorfer, C. E. Ansona, and A. K. Powell, *Dalt. Trans.*, 2009, 1901.
5. G. E. Kostakis, S. P. Perlepes, V. A. Blatov, D. M. Proserpio, and A. K. Powell, *Coord. Chem. Rev.*, 2012, **256**, 1246.
 6. (a) A. V Pali, B. S. Tsukerblat, E. Coronado, J. M. Clemente-Juan, and J. J. Borrás-Almenar, *J. Chem. Phys.*, 2003, **118**, 5566; (b) F. Lloret, M. Julve, J. Cano, R. Ruiz-Garcia, and E. Pardo, *Inorg. Chim. Acta*, 2008, **361**, 3432; (c) S. Ostrovsky, Z. Tomkowicz, and W. Haase, *Coord. Chem. Rev.*, 2009, **253**, 2363.
 7. N. Ishikawa, M. Sugita, T. Ishikawa, S. Koshihara, and Y. Kaizu, *J. Am. Chem. Soc.*, 2003, **125**, 8694.

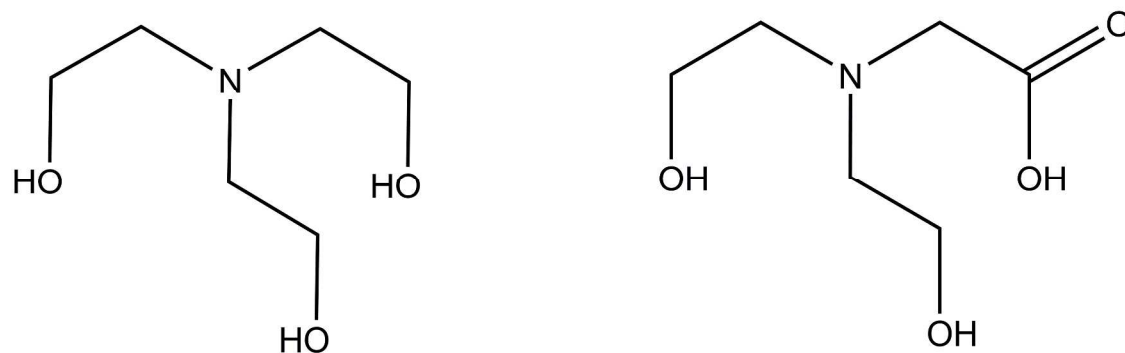
8. (a) J. M. Zadrozny and J. R. Long, *J. Am. Chem. Soc.*, 2011, **133**, 20732; (b) S. Mossin, B. L. Tran, D. Adhikari, M. Pink, F. W. Heinemann, J. Sutter, R. K. Szilagyi, K. Meyer, and D. J. Mindiola, *J. Am. Chem. Soc.*, 2012, **134**, 13651; (c) J. M. Zadrozny, J. Liu, N. a Piro, C. J. Chang, S. Hill, and J. R. Long, *Chem. Commun.*, 2012, **48**, 3927; (d) D.-K. Cao, J.-Q. Feng, M. Ren, Y.-W. Gu, Y. Song, and M. D. Ward, *Chem. Commun.*, 2013, **49**, 8863; (e) F. Yang, Q. Zhou, Y. Zhang, G. Zeng, G. Li, Z. Shi, B.-W. Wang, and S. Feng, *Chem. Commun.*, 2013, **49**, 5289; (f) J. M. Zadrozny, D. J. Xiao, M. Atanasov, G. J. Long, F. Grandjean, F. Neese, and J. R. Long, *Nat. Chem.*, 2013, **5**, 577; (g) E. Colacio, J. Ruiz, E. Ruiz, E. Cremades, J. Krzystek, S. Carretta, J. Cano, T. Guidi, W. Wernsdorfer, and E. K. Brechin, *Angew. Chem. Int. Ed. Engl.*, 2013, **52**, 9130; (h) J. M. Zadrozny, M. Atanasov, A. M. Bryan, C.-Y. Lin, B. D. Rekker, P. P. Power, F. Neese, and J. R. Long, *Chem. Sci.*, 2013, **4**, 125; (i) D. Wu, X. Zhang, P. Huang, W. Huang, M. Ruan, and Z. W. Ouyang, *Inorg. Chem.*, 2013, **52**, 10976; (j) Y.-Y. Zhu, C. Cui, Y.-Q. Zhang, J.-H. Jia, X. Guo, C. Gao, K. Qian, S.-D. Jiang, B.-W. Wang, Z.-M. Wang, and S. Gao, *Chem. Sci.*, 2013, **4**, 1802; (k) R. Ruamps, L. J. Batchelor, R. Guillot, G. Zakhia, A.-L. Barra, W. Wernsdorfer, N. Guihéry, and T. Mallah, *Chem. Sci.*, 2014, **5**, 3418; (l) R. Boča, J. Miklovič, and J. Titiš, *Inorg. Chem.*, 2014, **53**, 2367; (m) A. Eichhöfer, Y. Lan, V. Mereacre, T. Bodenstein, and F. Weigend, *Inorg. Chem.*, 2014, **53**, 1962.
9. (a) P. Alborés and E. Rentschler, *Dalton Trans.*, 2009, 2609; (b) P. Alborés and E. Rentschler, *Angew. Chem. Int. Ed. Engl.*, 2009, **48**, 9366; (c) I. C. Lazzarini, L. Carrella, E. Rentschler, and P. Alborés, *Polyhedron*, 2012, **31**, 779; (d) I. C. Lazzarini, A. V Funes, L. Carrella, L. Sorace, E. Rentschler, and P. Alborés, *Eur. J. Inorg. Chem.*, 2014, **2014**, 2561;
10. G. Aromi, A. S. Batsanov, P. Christian, M. Helliwell, A. Parkin, S. Parsons, A. A. Smith, G. A. Timco, and R. E. P. Winpenny, *Chem. Eur. J.*, 2003, **9**, 5142.
11. R. A. Coxall, S. G. Harris, D. K. Henderson, S. Parsons, P. A. Tasker, and R. E. P. Winpenny, *J. Chem. Soc. Dalton. Trans.*, 2000, 2349.
12. (a) A. E. Malkov, T. B. Mikhailova, G. G. Aleksandrov, E. V Pakhmutova, I. M. Egorov, A. A. Sidorov, I. G. Fomina, S. E. Nefedov, I. L. Eremenko, and I. I. Moiseev, *Russ. Chem. Bull.*, 2001, **50**, 2485; (b) T. C. Stamatatos, C. P. Raptopoulou, S. P. Perlepes, and A. K. Boudalis, *Polyhedron*, 2011, **30**, 3026; (c) E. Fursova, O.

- Kuznetsova, V. Ovcharenko, G. Romanenko, V. Ikorskii, I. L. Eremenko, and A. Sidorov, *Polyhedron*, 2007, **26**, 2079; (d) S. K. Langley, M. Helliwell, S. J. Teat, and R. E. P. Winpenny, *Dalton Trans.*, 2012, **41**, 12807; (e) A. Tsohos, S. Dionyssopoulou, C. P. Raptopoulou, A. Terzis, E. G. Bakalbassis, and S. P. Perlepes, *Angew. Chem.-Int. Ed.*, 1999, 983; (f) G. S. Papaefstathiou, S. P. Perlepes, A. Escuer, R. Vicente, and X. Solans, *Angew. Chem.-Int. Ed.*, 2001, **40**, 884; (g) Z.-Q. Jia, X.-J. Sun, L.-L. Hu, J. Tao, R.-B. Huang, and L. S. Zheng, *Dalton Trans.*, 2009, 6364.
13. A. Ferguson, A. Parkin, and M. Murrie, *Dalton Trans.*, 2006, 3627.
 14. N. F. Chilton, R. P. Anderson, L. D. Turner, A. Soncini, and K. S. Murray, *J. Comput. Chem.*, 2013, **34**, 1164.
 15. (a) P. Alborés and E. Rentschler, *Inorg. Chem.*, 2008, **47**, 7960; (b) P. Alborés, C. Plenk, and E. Rentschler, *Inorg. Chem.*, 2012, **51**, 8373; (c) P. Alborés, J. Seeman, and E. Rentschler, *Dalton Trans.*, 2009, 7660; (d) P. Alborés and E. Rentschler, *Dalton Trans.*, 2010, **39**, 5005; (e) I. C. Lazzarini, L. M. Carrella, E. Rentschler, and P. Alborés, *Polyhedron*, 2011, **31**, 779; (f) P. Alborés and E. Rentschler, *Dalton Trans.*, 2009, **2**, 2609.
 16. (a) A. Ferguson, M. Schmidtman, E. K. Brechin, and M. Murrie, *Dalton Trans.*, 2011, **40**, 334; (b) V. Tudor, A. Madalan, V. Lupu, F. Lloret, M. Julve, and M. Andruh, *Inorg. Chim. Acta*, 2010, **363**, 823; (c) L.-L. L. Hu, Z.-Q. Q. Jia, J. Tao, R.-B. B. Huang, and L. S. Zheng, *Dalton Trans.*, 2008, 6113; (d) T. Shiga and H. Oshio, *Polyhedron*, 2007, **26**, 1881; (e) M. Moragues-Canovas, C. E. Talbot-Eeckelaers, L. Catala, F. Lloret, W. Wersndorfer, E. K. Brechin, and T. Mallah, *Inorg. Chem.*, 2006, **45**, 7038.
 17. A. Abraham and B. Bleaney, *Electron Paramagnetic Resonance of Transition Ions*, Oxford University Press, 1970.
 18. A. H. Morrish, *The Physical Principles of Magnetism*, IEEE Press, New York, 2001.
 19. S. Stoll and A. Schweiger, *J. Magn. Reson.*, 2006, **178**, 42.
 20. SCALE3 ABSPACK: Empirical absorption correction, CrysAlis – Software package, Oxford Diffraction Ltd., Oxford, 2006.
 21. A. Altomare, M. C. Burla, M. Camalli, G. L. Cascarano, C. Giacovazzo, A. Guagliardi, A. G. G. Moliterni, G. Polidori, and R. Spagna, *J. Appl. Crystallogr.*, 1999, **32**, 115.
 22. Sheldrick, G. M., *Acta Cryst. A*, 2008, **64**, 112.
 23. L. J. Farrugia, *J. Appl. Crystallogr.*, 2012, **45**, 849.

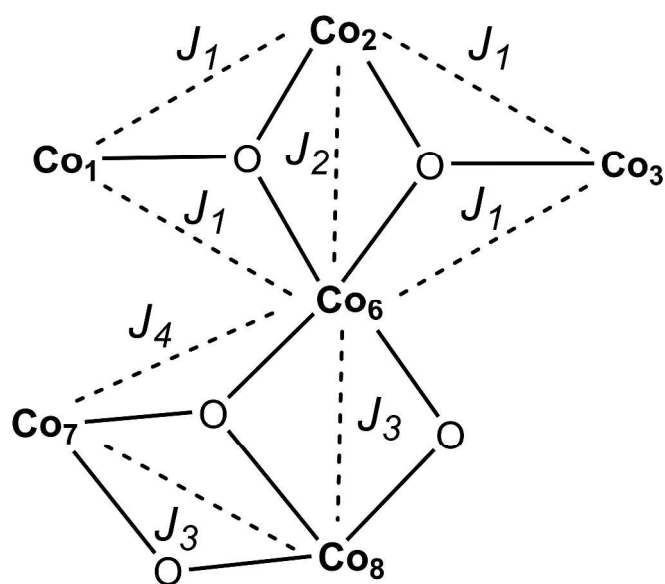
24. G. te Velde, F. M. Bickelhaupt, E. J. Baerends, C. Fonseca Guerra, S. J. A. van Gisbergen, J. G. Snijders, and T. Ziegler, *J. Comput. Chem.*, 2001, **22**, 931.
25. L. Noodleman, *J. Chem. Phys.*, 1981, **74**, 5737.
26. L. Noodleman and E. J. Baerends, *J. Am. Chem. Soc.*, 1984, **106**, 2316.
27. O. Kahn, *Molecular Magnetism*, VCH, New York, 1993.
28. E. Ruiz, J. Cano, S. Alvarez, and P. Alemany, *J. Comput. Chem.*, 1999, **20**, 1391.

Table 1. Experimental and DFT calculated exchange interaction parameters values for compound **1**.

	Exp./ cm^{-1}	DFT calcd./ cm^{-1}
$J_{\text{Co1-Co6}} (J_1)$	-5.9±0.2	-7.6
$J_{\text{Co1-Co2}} (J_1)$		-9.0
$J_{\text{Co2-Co3}} (J_1)$		-2.8
$J_{\text{Co3-Co6}} (J_1)$		-11.4
$J_{\text{Co2-Co6}} (J_2)$		6.6
$J_{\text{Co6-Co8}} (J_3)$	-1.5±0.1	-1.2
$J_{\text{Co7-Co8}} (J_3)$		-4.2
$J_{\text{Co6-Co7}} (J_4)$		2.9



Scheme 1. Molecular sketches of the teaH₃ (left) and bicH₃ (right) ligands.



Scheme 2. Spin topology of compound **1** with the approximate exchange interaction pattern proposed.

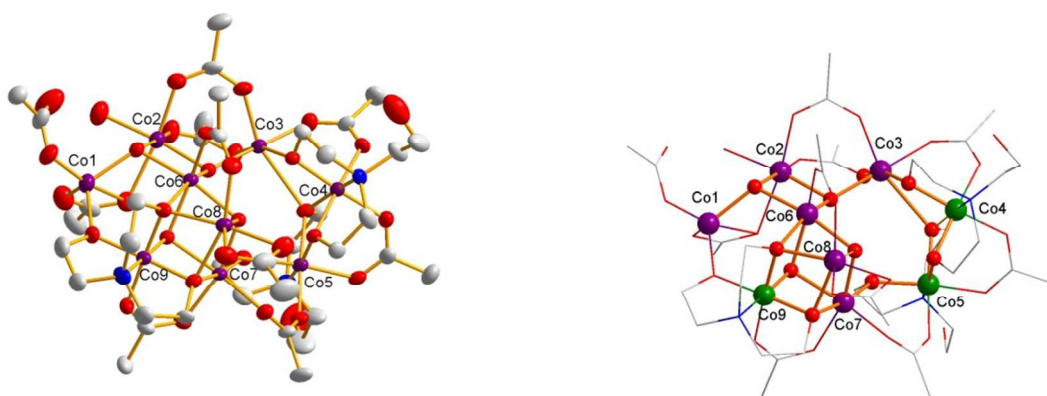


Figure 1. Left: Molecular representation of compound **1**. Hydrogen atoms and *tert*-butyl groups have been omitted for sake of clarity. Ellipsoids drawn at 30% probability level. Violet: cobalt; Red: oxygen; Blue: nitrogen; Gray: carbon. Right: $\{\text{Co}^{\text{II}}_6\text{Co}^{\text{III}}_3\}$ core. Violet: Co(II); Green: Co(III).

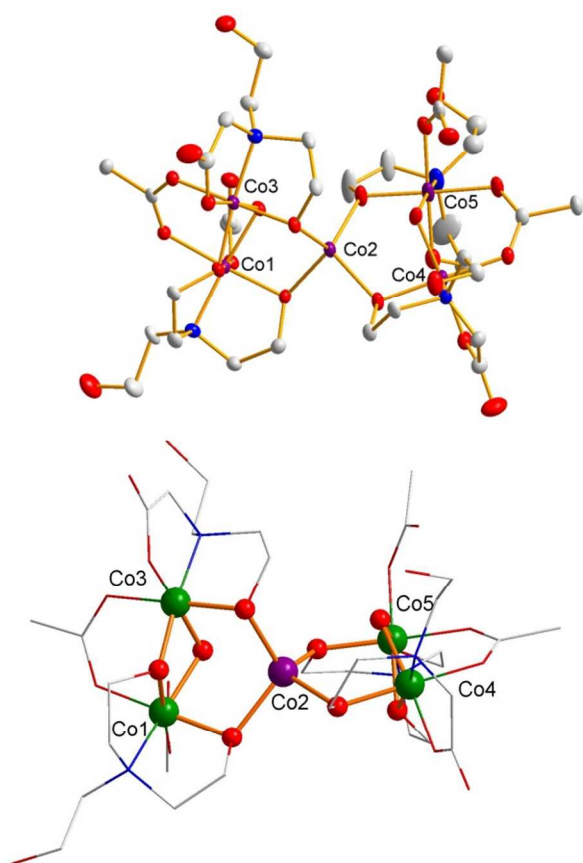


Figure 2. Left: Molecular representation of compound **2**. Hydrogen atoms and *tert*-butyl groups have been omitted for sake of clarity. Ellipsoids drawn at 30% probability level. Violet: cobalt; Red: oxygen; Blue: nitrogen; Gray: carbon. Right: $\{\text{Co}^{\text{II}}\text{Co}^{\text{III}}_4\}$ core. Violet: Co(II); Green: Co(III).

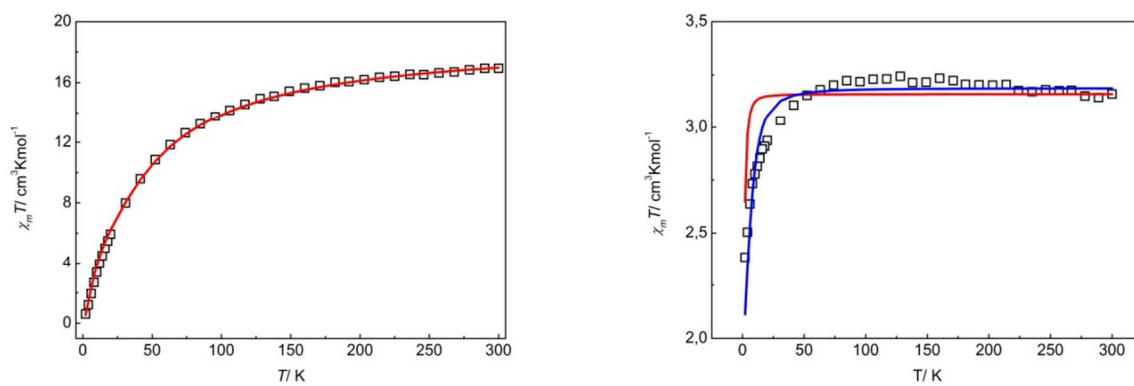


Figure 3. $\chi_m T$ vs T data plot at 1kOe in 2-300K range. Left: Compound **1**. Squares: experimental; Full line: fitted (see Table 1). Right: Compound **2**. Squares: experimental; Full line: fitted, red: $\chi_m T + MH$ simult.; blue: $\chi_m T$ only.

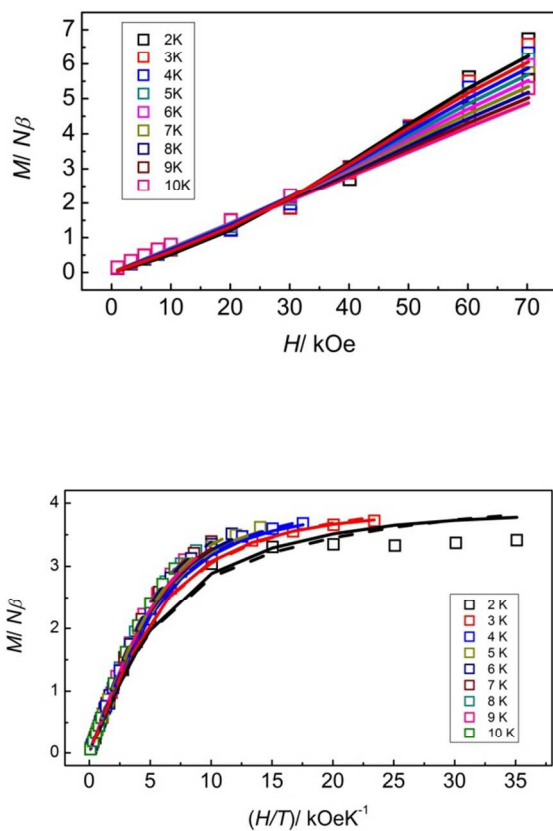


Figure 4. Top: M vs H data plot in the range 0-70 kOe and 2-10K of compounds **1**. Squares: experimental; full line: fitted. Bottom: and M vs H/T data plot in the range 0-70 kOe and 2-10K of compound **2** (bottom). Squares: experimental; full line: fitted ($\chi_m T + MH$) simult; dashed line: fitted (MH only).

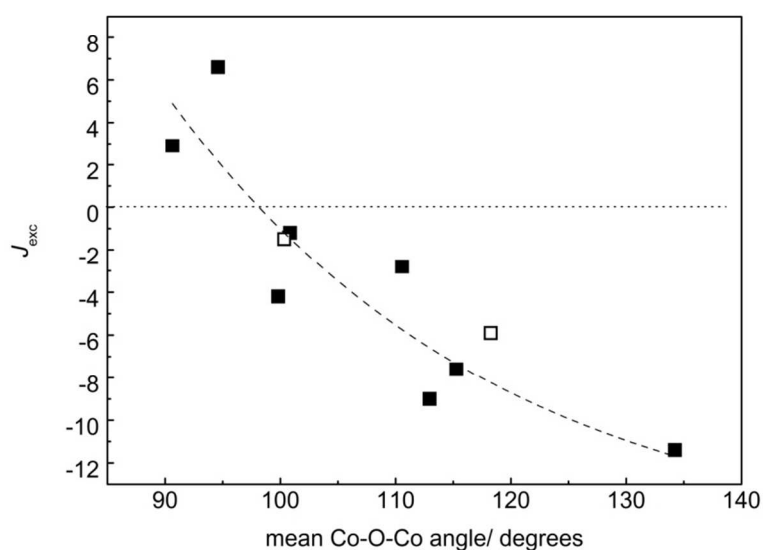


Figure 5. DFT based magneto-structural correlation between exchange interactions parameters in compound **1** and Co-O-Co angle. Full squares: DFT calculates values; Open squares: experimental fitted values; Dashed line: empirical correlation function.

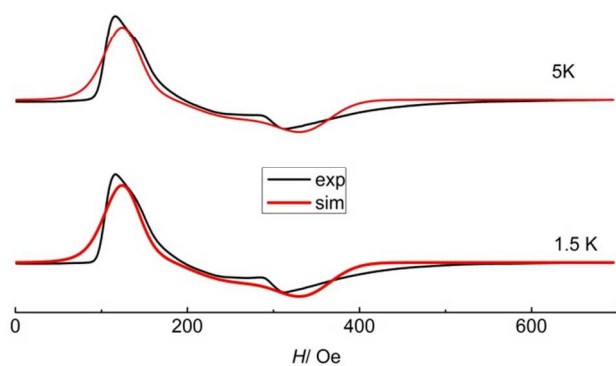


Figure 6. Powder X-band EPR spectra at 1.5 and 5 K of compound **2**. Simulation linewidth: 250 Oe; g -strain: [0.3,0.2,0.3]; H -strain/ Oe: [2100, 700, 430].

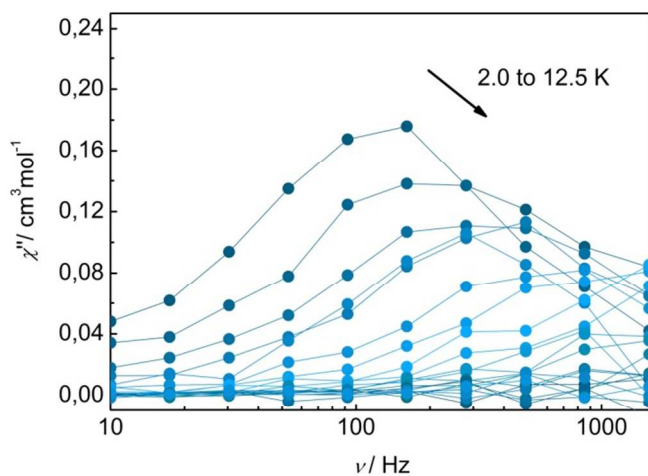


Figure 7. Compound **2** χ_m'' vs driving frequency (logarithmic scale), 0-1500 Hz (driving field 3 Oe) plot, in the range 2-12.5 K under a 2600 Oe DC applied field.

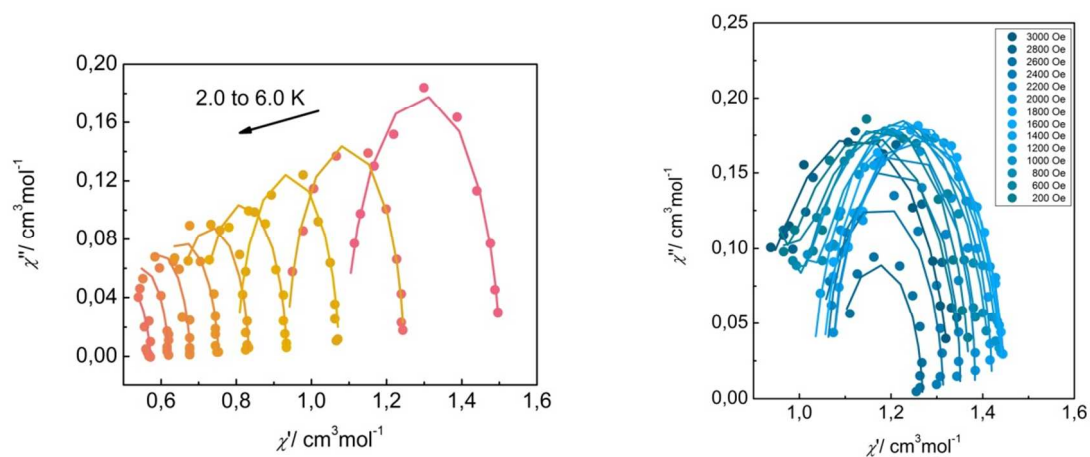


Figure 8. Left: Cole-Cole plot at 1400 Oe DC applied field of compound **2**, in the 2-6 K range. Right: Cole-Cole plot at 2K of compound **2**, in the 200-3000 Oe DC external field range. Circles: experimental data; Lines: best fitting (see Text).

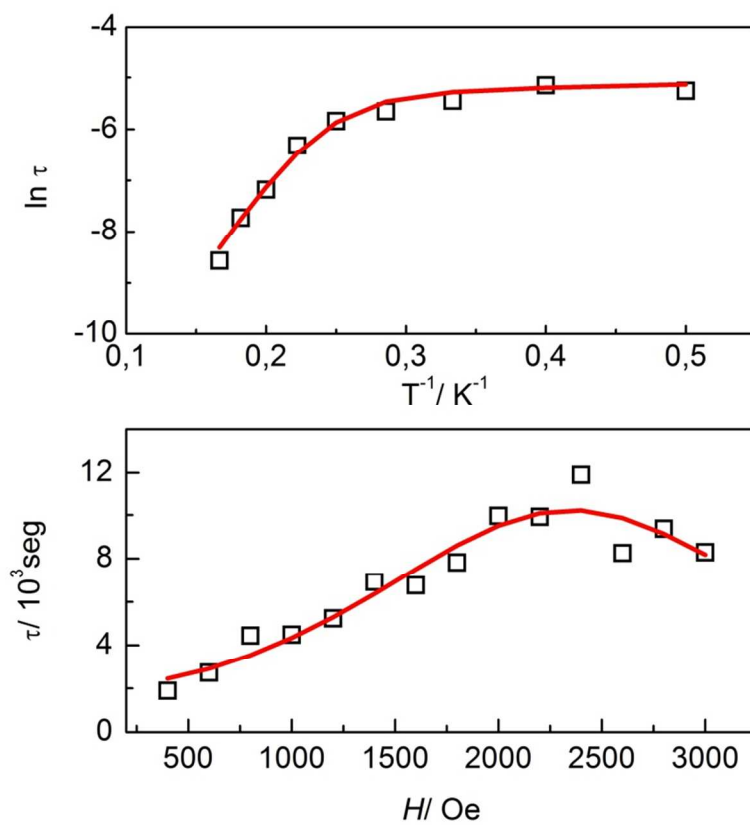


Figure 9. Top: Arrhenius type plot for the T dependence of the characteristic relaxation time at 2600 Oe DC external field for compound **2**. Bottom: Field dependence of the characteristic relaxation time at 2K for compound **2**. Squares: experimental data; Full lines: best fitting curves (see Text).